# Fluorescence Characterization of the Transfer RNA-like Domain of Transfer Messenger RNA in Complex with Small Binding Protein B

**ARTICLE** *in* BIOCHEMISTRY · APRIL 2012

Impact Factor: 3.02 · DOI: 10.1021/bi201751k · Source: PubMed



**2 AUTHORS:**

May Daher
University of Michigan
**1** PUBLICATION **2** CITATIONS
SEE PROFILE

David Rueda
Imperial College London
**57** PUBLICATIONS **1,465** CITATIONS
SEE PROFILE

Published in final edited form as:
*Biochemistry*. 2012 May 1; 51(17): 3531–3538. doi:10.1021/bi201751k.

# Fluorescence Characterization of the tRNA-like Domain of tmRNA in Complex with SmpB

**May Daher Farhat** and **David Rueda***
Department of Chemistry, Wayne State University, MI 48202

## Abstract

tmRNA and SmpB are the main components of the trans-translation rescue machinery that releases stalled ribosomes from defective mRNAs. Little is known about how SmpB binding affects the conformation of the tRNA-like domain (TLD) of tmRNA. It has been previously hypothesized that the absence of a D-stem in the TLD provides flexibility in the elbow region of tmRNA, which can be stabilized by its interaction with SmpB. Here, we have used fluorescence Förster resonance energy transfer (FRET) to characterize the global structure of the tRNA-like domain of tmRNA in the presence and absence of SmpB and as a function of [$Mg^{2+}$]. Our results show tight and specific binding of SmpB to tmRNA. Surprisingly, our data shows that the global conformation and flexibility of tmRNA does not change upon SmpB binding. However, $Mg^{2+}$ ions induce an 8 Å compaction in the tmRNA structure, suggesting that the flexibility in the H2a stem may allow different conformations of tmRNA as the tRNA like domain (TLD) and mRNA like domain (MLD) need to be positioned differently while moving through the ribosome.

Defective or truncated messenger RNAs (mRNAs) lacking stop codons lead to ribosome stalling on the end of the message. Stalled ribosomes can cause two major problems for the cell: production of incomplete, non-functional and potentially toxic proteins, and depletion of the ribosomal pool available for translation.[1,2] In bacteria, these problems can be solved by a rescue process called trans-translation, which employs the hybrid transfer-messenger RNA (tmRNA) and its highly conserved cofactor, small protein B (SmpB).[3,4] These two factors are universally conserved in bacterial species and trans-translation is important for a wide variety of physiological processes, including gene expression, pathogenesis, and response to stress, making tmRNA an attractive target for antibacterial drug discovery.[1,5] Indeed, Pyrazinamide, a first-line tuberculosis drug, acts by inhibiting the ribosome rescue pathway.[6]

Transfer-messenger RNA consists of two domains (Figure 1A): the tRNA-like domain (TLD) and the mRNA-like domain (MLD). The TLD includes an acceptor stem and a TΨC arm (Figure 1A,B). However, in lieu of a D arm, it contains an irregular D loop without predicted helical pairing, and instead of an anticodon loop it contains an irregular helix (H2a) that joins the TLD to the MLD through four pseudoknots (pk1–pk4, Figure 1AB). The MLD comprises an open reading frame that encodes for a protein tag that signals for degradation of the incomplete protein.[3,7–9] Transfer-messenger RNA enters into the A site of stalled ribosomes with its TLD in complex with SmpB and the elongation factor EF-Tu.[3] In the A site, the nascent peptide chain is transferred to the TLD, which translocates into the P site releasing the defective mRNA. Then, the first codon of the MLD enters the decoding center, where it is translated by normal aminoacyl-tRNAs. The resulting peptide tag is

*Author to whom correspondence should be addressed: david.rueda@wayne.edu, Tel.: (313) 577-6918, Fax: (313) 577-8822.

Supplementary Materials. Quantum yield and $R_0$ determination for each construct, trFRET results and average fluorescein excited state lifetimes. This material is available free of charge via the Internet at http://pubs.acs.org.

recognized by specific cellular proteases that degrade the defective protein.[1,8,10] All of these steps require a special set of interactions between tmRNA, SmpB, the ribosome and the translational cofactors.[11]

A transient electric birefringence (TEB) study of the tmRNA TLD in absence of SmpB has revealed a more obtuse angle (110° instead of 90°) between the acceptor and helix H2a stems compared to canonical tRNAs.[12] This has been confirmed in the crystal structure of the TLD-SmpB complex, which revealed an obtuse angle of 120° between the acceptor stem and the helix H2a, but a 90° angle between the acceptor stem and SmpB.[13] Based on this result, the authors hypothesized that SmpB mimics a canonical acceptor stem and interacts with the decoding site, while the H2a arm functions as a class II tRNA long variable arm. More recently, interactions between SmpB and the decoding site have supported this hypothesis.[14,15]

It has been previously hypothesized that the lack of a D-stem in the TLD may provide flexibility in the elbow region of tmRNA, between H2 and the acceptor arm, which can be stabilized by its interaction with SmpB.[16] This is an important question because it affects the possible tmRNA conformations during tmRNA accommodation and how the MLD is introduced into the decoding center while the aminoacyl group resides in the peptidyl transferase center. In particular, it is not yet known whether SmpB or $Mg^{2+}$ ions modulate the TLD domain structure. To address this question, we have used fluorescence anisotropy and FRET to measure the distance between the acceptor and the H2a stem in the presence and absence of SmpB. We also compare our results to a canonical tRNA and a mitochondrial tRNA (mtRNA) that lacks the D-stem. Surprisingly, our data show that the global conformation and flexibility of the TLD does not change upon SmpB binding. However, $Mg^{2+}$ ions induce an 8 Å compaction of the TLD.

## MATERIALS AND METHODS

### RNA purification and fluorophore labeling

RNA strands were purchased from the Keck Foundation Biotechnology Resource Laboratory at Yale University School of Medicine (New Haven, CT). RNAs were constructed using two strands: A 5′ strand containing the D-loop, and a 3′ strand containing the T arm (sequences in Figure 1). The 5′ strands were labeled with a 5′ fluorescein and a 3′ amino linker (Figure 1). RNA strands were deprotected, purified and labeled with a 3′ tetramethylrhodamine (TMR) as described.[17] The location of the fluorophores (top of acceptor stem and bottom of H2a helix, Figure 1) was chosen far from the SmpB binding site (elbow region) to minimize the possibility of affecting SmpB binding.

### SmpB expression and purification

SmpB protein cloning and expression was performed as previously described.[16] Plasmid containing the *smpB* gene with C- terminal histidine-tag (pET21) was obtained from N. Ban (Institute of Molecular Biology and Biophysics, ETH, Zurich, Switzerland). The gene was transformed into *E. coli* BL21/DE3. Histidine-tagged SmpB was bound to a nickel column (IMAC column), washed and eluted with 250 mM imidazole (300 mM NaCl, 50 mM $Na_2HPO_4$, pH 8.0).[16] A 12% SDS-acrylamide gel was used to check the protein purity. Pure fractions were dialyzed against storage buffer (20 mM NaCl, 10 mM $Na_2HPO_4$, pH 6.5). The protein concentration was measured using UV-VIS absorbance at 280 (extinction coefficient = 22,900 $M^{-1}cm^{-1}$).

### Anisotropy measurements

Fluorescence anisotropy measurements were performed using a spectrofluorometer with automated polarizers (Varian, Carry Eclipse). Fluorescein-only labeled 5′ strand (25 nM) and 3′ strand (50 nM) were heated at 90°C for 2 min and annealed >15 min at room temperature in standard buffer (50 mM Tris-HCl, pH 7.5, 100 mM NaCl, 1 mM $MgCl_2$). Fluorescence anisotropy was studied in the presence of the donor fluorophore alone, because Fluorescence Energy Transfer can result in a decrease of the donor fluorescence intensity, thus compromising our ability to measure fluorescence anisotropy and interpreting the results. Measurements were performed at room temperature at RNA:protein ratios varying from 1:0.0004 to 1:4. Fluorescein was excited at 490 nm (5 nm bandwidth), parallel ($I_{//}$) and perpendicular ($I_{\perp}$) emission intensities were measured at 520 nm (5 nm bandwidth).[18–20]

Fluorescence anisotropy was calculated as, $r(t)=\frac{I_{\perp}-GI_{//}}{I_{\perp}+2GI_{//}}$, where $G$ is an empirically determined, instrument dependent correction factor. The data were fit to the quadratic binding equation assuming 1:1 stochiometry,

$$f(SmpB)=r_0+(r_{\max}-r_0)\frac{\left((K_D+[RNA_0]+[SmpB])-\sqrt{(K_D+[RNA_0]+[SmpB])^2-(4[RNA_0][SmpB])}\right)}{2\times[RNA_0]}$$

where $r_0$ and $r_{max}$ are the fluorescence anisotropies of fluorescein labeled tmRNAΔ alone and bound to SmpB, respectively, $K_D$ is the dissociation constant, [$RNA_0$] is the initial RNA concentration (25 nM) and [SmpB] is the total (free + bound) SmpB concentration. Control anisotropy experiments by direct excitation of TMR labeled tmRNAΔ confirm that the binding affinity remains in the low nanomolar range and that neither the free aminolinker nor TMR affect SmpB binding to tmRNAΔ (Supp. Fig. 1).

### Steady State FRET (ssFRET) measurements

FRET measurements were carried out using a spectrofluorometer (Varian Carry Eclipse), as described.[17,21–24] Doubly labeled (Fluorescein-TMR) 5′ strand (25 nM) and 3′ strand (50 nM) were heated and annealed as described above. The experiments were performed at room temperature. Fluorescein was excited at 490 nm (10 nm bandwidth). Fluorescein and TMR emissions were measured at 520 nm and 580 nm (5 nm bandwidth), respectively. The apparent FRET efficiency was calculated as $FRET=I_{580}/(I_{580}+I_{520})$, where $I_{520}$ and $I_{580}$ are the fluorescein and TMR emission intensities, respectively. SmpB was titrated from 0.01 nM to 100 nM. For each measurement, the solution was manually mixed and allowed to incubate for 5 minutes before recording the emission spectra.

### Time-resolved FRET (trFRET) measurements

To determine the end-to-end distance distribution of tmRNAΔ, we used trFRET, as described.[17,21,25] A 250 nM solution of labeled 5′ strand (fluorescein-only or fluorescein-TMR labeled) and 500 nM of 3′ strand was heated and annealed as described above. Fluorescein was excited at 490 nm (30 nm bandwidth dichroic filter) with a Yb-doped fiber laser (5 ps pulses, 40 MHz). Donor emission was collected at 520 nm (20 nm bandwidth dichroic filter) using a micro channel photomultiplier tube (R3890U-52, Hamamatsu) feeding a time-correlated single photon counting card (SPC-630, Becker & Hickl) under magic angle polarization (54.7°) to more than 40,000 peak counts. Fluorescence decays were collected in 4816 channels with 12.2 ps/channel time resolution. A dilute non-dairy coffee creamer solution was used to measure the instrument function. The decay of the donor

emission in the absence and the presence of the acceptor and with and without SmpB were collected under identical conditions. The time-resolved for the donor only complex was used to extract the three intrinsic parameters, donor lifetimes $\tau_i$, fractional contributions $\alpha_i$, and $\mu_i$, The data from the doubly labeled tRNAΔs ($I_{DA}$) were then fitted according to the following equation:

$$I_{DA}(t)=I_0\int P(R)\sum_i \alpha_i \exp\left(-\frac{t}{\tau_i}\left[1+\left(\frac{R_0}{R}\right)^6\right]\right)dR,$$

where $I_0$, is the initial intensity, $\tau_i$ and $\alpha_i$, are the singly labeled lifetime, and the corresponding decay amplitude parameters respectively, *P(R)* is the distance distribution, $R_0$ is the Förster distance for 50 % energy transfer (independently determined for the fluorescein-TMR FRET pair for each construct, see Supplementary Materiasl)[17,21,25–27]. The distance distribution *P(R)* was analyzed as a three-dimensional weighted Gaussian:

$$P(R)=4\pi R^2 N\exp\left(-(R-\mu)^2/\sigma^2\right),$$

where $N$ is a normalization constant, and $\sigma$ and $\mu$ describe the shape of the Gaussian. An additional parameter was the fraction of singly labeled RNA since the labeling reaction could not be 100% efficient. The ability to quantify multiple populations, including singly labeled RNA, has been well established previously[17,21,25–28]. This equation gives information about the mean distance between the fluorescein and TMR, the distance distribution indicates the conformational flexibility of the complex, and the fractional population provides information about the basis for the thermodynamic analyses of conformational equilibrium.[17,21] To test the effect of SmpB and $Mg^{2+}$ on the fluorescein, we measured its quantum yield (QY) and the average excited lifetime for each fluorescein-only construct in the absence and in the presence of SmpB, and in the absence and presence of $Mg^{2+}$ (Supplementary Materials). The data show that, within the standard deviation, both the QY and the average excited state lifetime remain constant for all constructs under our conditions.

## RESULTS

### SmpB binds tmRNAΔ tightly and specifically

First, we sought to confirm that SmpB efficiently binds the fluorophore-labeled tmRNAΔ construct using fluorescence anisotropy. Fluorescence anisotropy is a dimensionless quantity (r) that measures the rotation of a fluorophore. Low fluorescence anisotropies indicate that the fluorophore tumbles freely in solution, whereas high anisotropies indicate that the fluorophore rotation is hindered, for example by the formation of a large molecular weight complex.[19] In the absence of protein, the observed anisotropy value for tmRNAΔ alone is low (0.06 ± 0.01). In the presence of 100 nM SmpB, the anisotropy increases to 0.15 ± 0.03, indicating that a larger molecular weight protein-RNA complex is formed. A protein titration from 0.01 to 100 nM (Figure 2) shows that the observed anisotropy values increase smoothly from 0.06 to 0.15. A fit to the quadratic equation (see Materials and Methods) results in a dissociation constant $K_D$ = 1.0 ± 0.1 nM, comparable to previously reported values.[8] This result shows that SmpB binds tightly to our fluorophore-labeled tmRNAΔ construct with one-to-one stochiometry.[8]

To test for the specificity of the protein binding, we repeated the experiments using fluorophore-labeled alanyl tRNA (tRNAΔ, Figure 1) and mitochondrial seryl tRNA (mtRNAΔ, Figure 1), which are not expected to bind SmpB. The corresponding titrations

show that the fluorescence anisotropy of both RNAs remains low (0.07 ± 0.01) throughout the protein concentration range, indicating that SmpB does not bind tRNAΔ or mtRNAΔ. These data are consistent with previous results that show that SmpB binds tRNA with a 400-fold higher dissociation constant than tmRNA.[8] Our data suggests that only one SmpB binds the TLD, in agreement with prior studies,[13,16] but in contradiction with one other study that suggests that multiple SmpB molecules can bind the TLD.[29]

Overall, the fluorescence anisotropy data show that SmpB binds tmRNAΔ tightly, specifically and stochiometrically.

## $Mg^{2+}$ but not $Na^{+}$ ions inhibit SmpB binding

We then sought to study the effect of monovalent and divalent cations on tmRNA-SmpB binding. We repeated the fluorescence anisotropy titration (Figure 2) in 0, 1 and 10 mM $Mg^{2+}$ concentration, and in the presence of 20 or 100 mM $Na^{+}$. Figure 3 shows the resulting SmpB dissociation constants ($K_D$) under these conditions. In the absence of Mg2+ and in 100 mM $Na^{+}$, the dissociation constant is 0.4 ± 0.1 nM. Increasing the $Mg^{2+}$ concentration to 1 and 10 mM increases the dissociation constant to 1.0 ± 0.1 nM and 2.6 ± 0.6 nM, respectively. These results show that $Mg^{2+}$ ions has an inhibitor effect on SmpB binding.

When the sodium concentration is dropped to 20 mM (Figure 3B), the binding dissociation constant ranges from 2.7 ± 1.0 nM (in the absence of $Mg^{2+}$) to 11 ± 5 nM (in 10 mM $Mg^{2+}$), between 4- and 8-fold higher than in 100 mM $Na^{+}$. The fact that SmpB binds better at the higher concentration of $Na^{+}$ might be due to increased tmRNAΔ tertiary structure stability that in turn stabilizes SmpB binding. Regardless of the cause, this result shows that the $Mg^{2+}$ inhibition of SmpB binding is specific and not solely electrostatic in nature. Overall, these results indicate that $Mg^{2+}$ ions inhibit SmpB binding on tmRNAΔ and that high $Na^{+}$ ion concentrations are required for tight SmpB binding.

## SmpB does not induce global conformational changes in tmRNAΔ

To monitor the global structure of tmRNAΔ upon SmpB binding, we used steady state FRET (ss-FRET), which measures the apparent energy transfer efficiency from an excited donor fluorophore to an acceptor fluorophore in close proximity. The apparent FRET efficiency is extremely sensitive to the distance between the fluorophores in the 2–8 nanometer range, thus FRET measurements can be a valuable tool for probing molecular structure and interactions.[30] We placed the fluorophores fluorescein and tetramethylrhodamine at the ends of the acceptor and helix H2a, respectively (Figure 1A) to detect any conformational changes that would alter the angle between the acceptor stem and the H2a arm. High FRET efficiency indicates that the two fluorophores are in close proximity, and therefore, a more acute angle between the helices, whereas low FRET efficiency indicates a longer distance between the two fluorophores, and therefore, a more obtuse angle between the helices. In the absence of SmpB, the observed apparent FRET efficiency is 0.23 ± 0.02 (Figure 4).

In the presence of 0.01 to 100 nM SmpB, the observed apparent FRET efficiency remains approximately constant, indicating that the global tmRNAΔ conformation remains unchanged. FRET can only report on the tmRNAΔ global conformation, and therefore, our experiments cannot rule out local conformational changes at the binding site of the protein. Control experiments with tRNAΔ and mtRNAΔ, which do not bind SmpB, also show no changes in apparent FRET efficiency in the presence of 0.01 to 100 nM SmpB (Figure 4). Comparison of the observed FRET efficiencies reveals interesting structural differences between tmRNAΔ, tRNAΔ and mtRNAΔ. The lowest observed apparent FRET efficiency (0.20 ± 0.02) corresponds to tRNAΔ, indicating that it has the longest distance between the

acceptor stem and anticodon stem. The highest apparent FRET efficiency (0.28 ± 0.01) corresponds to mtRNAΔ, indicating that it has the shortest distance between the acceptor stem and anticodon stem. The tmRNAΔ apparent FRET efficiency (0.23 ± 0.02) lies in between. Based on the crystal structure and the TEB studies, one would expect tmRNAΔ to have lower apparent FRET efficiency than tRNAΔ, in apparent contradiction with these results. A possible explanation is that the acceptor stem of tmRNAΔ rotates around its helical axis (relative to tRNAΔ) to bring the 5′ end closer to the H2a arm.

ssFRET provides only an average apparent FRET efficiency and may not detect the presence of minor populations in solution. To measure the distribution of distances between the acceptor stem and helix H2a in the tmRNAΔ-SmpB complex, we used time resolved FRET (trFRET). trFRET consists of measuring the fluorescence lifetime of the donor fluorophore in absence and presence of the acceptor (Figure 5A, top panel). Energy transfer from the excited donor to the acceptor results in an apparent decrease in the donor fluorescence lifetime (compare black and green curves), which can be used to determine the distribution of distances between the fluorophores (Figure 5A bottom panel, green, Materials and Methods). In the absence of SmpB, the resulting distribution for tmRNAΔ reveals a bimodal distribution. The major component (~70%, centered at 60 ± 1 Å) is assigned to the complex formed by the 5′ and 3′ strands, whereas the minor component (~30%, centered at 29 ± 1 Å) is assigned to a hairpin RNA formed by the 5′ strand alone. Control experiments in the absence of the 3′ strand (not shown), confirm these assignments. The bimodal distribution is confirmed by the reduced Chi-square ($\chi^2 \leq 1.2$) compared to a single distribution fit ($\chi^2 \geq 1.4$).[19,31] In the presence of SmpB, tmRNAΔ displays an almost identical distribution with a major component (~70%, centered at 61 ± 1 Å), and a minor component (~30%, centered at 29 ± 1 Å). This result confirms that the interaction between SmpB and tmRNAΔ does not change the distance between the acceptor stem and the helix H2a of tmRNAΔ.

We repeated the experiments with the canonical tRNAΔ, which does not bind SmpB (Figure 5B). The resulting distributions (bottom panel) show that, in the absence of SmpB (green), the major component is centered at 67 ± 1 Å, 5 Å longer than tmRNAΔ, in agreement with the ssFRET data (Figure 4). In the presence of SmpB (red), the major distribution remains unchanged, as expected. Similar results were observed with mtRNAΔ (Figure 5C), except that the distance between the acceptor stem and the anticodon stem is ~ 6 Å shorter than tmRNAΔ, in agreement with the ssFRET data (Figure 4). Overall, these results show that SmpB does not change the overall conformation of tmRNAΔ upon binding. A comparison of the results for tmRNAΔ, tRNAΔ and mtRNAΔ reveals that, in 1 mM $Mg^{2+}$, the distance distributions between the acceptor stem and the helix H2a of tmRNAΔ lies between those observed for the control RNAs.

## $Mg^{2+}$ ions compress the tmRNAΔ structure

To determine the effect of divalent ions on the global conformation of tmRNAΔ, we used trFRET to measure the distance distributions from the acceptor stem to H2a between 0.1 mM and 100 mM $Mg^{2+}$ ions (Figure 6). In the absence of protein and in 0.1 mM $Mg^{2+}$, the mean distance between the two fluorophores is 62 ± 1 Å for tmRNAΔ (Figure 6A), two angstroms longer than in 1 mM $Mg^{2+}$. This distance decreases smoothly to reach 55 ± 1 Å above 10 mM $Mg^{2+}$. A fit to the quadratic equation yields a dissociation constant $K_{Mg}$ = 2.2 ± 0.6 mM.

In the presence of SmpB and 0.1 mM $Mg^{2+}$, the distance between the two fluorophores is 64 ± 1 Å, four angstroms longer than in 1 mM $Mg^{2+}$. The distance also decreases with increasing magnesium concentrations to reach 55 ± 1 Å above 10 mM (Figure 6B). A fit to the quadratic equation also results in a dissociation constant $K_{Mg}$ = 2.0 ± 0.9 mM. These results are within experimental error of the distance measured in the absence of SmpB,

confirming that SmpB binding does not induce global conformational changes in tmRNAΔ upon binding. This result seems in apparent contradiction with our previous result showing that $Mg^{2+}$ has an inhibitor effect on the binding site of the protein (Figure 2). However, previous studies have shown that $Mg^{2+}$ ions have multiple binding sites with different binding affinities on tRNA.[32] Therefore, a possible explanation for this result is that two distinct $Mg^{2+}$ ions are involved: one that has an inhibitor effect on the binding site of SmpB, while the other may bind inside the elbow region and results in the structural compaction of tmRNAΔ.

Unlike tmRNAΔ, the mean distance between the fluorophores in tRNAΔ remains constant at 66 ± 1 Å at all magnesium concentrations above 0.1 mM, suggesting that all $Mg^{2+}$ ions are already tightly bound in the low concentration range. This is consistent with previous studies that showed that magnesium can stabilize tRNA tertiary structure in the micromolar range.[33] The presence of SmpB does not change the observed mean distance, as expected.

Mitochondrial tRNAΔ behaves similar to tmRNAΔ. In the absence of SmpB and in low magnesium, the observed mean distance is 56 ± 1 Å, and this decreases slightly to 53 ± 1 Å above 10 mM magnesium (Figure 6). A fit to the quadratic equation yields a dissociation constant $K_{Mg}$ = 0.5 ± 0.3 mM, in agreement with a previously reported value.[34] This result suggests that the observed compaction for tmRNAΔ and mtRNAΔ may both be related to the absence of a D arm.

Overall, comparing the $Mg^{2+}$ titration between tmRNAΔ, tRNAΔ and mtRNAΔ suggests that the lack of a D-stem (tmRNAΔ and mtRNAΔ) results in a low millimolar affinity $Mg^{2+}$ binding site that causes the distance between the acceptor stem and H2a to decrease, but that does not compete for SmpB binding. Our data is in agreement with TEB data that showed a more acute angle in the presence of magnesium than in the absence of magnesium at 4°C.[12]

## DISCUSSION

Transfer-messenger RNA and SmpB are two of the key components in the bacterial ribosome rescue system, and the interaction between these two molecules is necessary for entry into stalled ribosomes.[35] Previous studies have suggested that SmpB mimics the anticodon loop of canonical tRNA, and binds to the decoding center of the ribosome, whereas the helix H2a functions as a long variable arm of class II tRNAs.[13,14] To determine the effect of SmpB and $Mg^{2+}$ ion binding on the structure and dynamics of tmRNA, we designed a fluorophore-labeled construct (tmRNAΔ) that is very similar to the construct used in a previous crystallographic study.[16] The fluorescence anisotropy data confirms that SmpB binds tmRNAΔ tightly and specifically. We then used steady state and time resolved FRET to monitor global conformational changes that would alter the angle between the acceptor stem and H2a of the tmRNAΔ upon interacting with SmpB. The results show no global conformational changes upon SmpB binding, suggesting that the angle between the acceptor step and H2a is more obtuse than that of canonical tRNAs, even in the absence of SmpB.

To fit into the ribosomal A site, canonical tRNAs must have a fixed distance between the decoding and the peptidyl transferase centers. But our trFRET measurements show that, at saturating $Mg^{2+}$ concentrations, the distance between the acceptor stem and the helix H2a in tmRNAΔ is ~8 Å shorter than in tRNAΔ in spite of the more obtuse angle (Figure 7A). Although a larger distance may be expected for tmRNA due to the larger angle, this result can be explained by rotation of the acceptor stem around the helical axis that brings the two ends closer. Indeed such a rotation is observed in the TLD-SmpB complex crystal structure (Figure 7A, compare left and middle).[13] The distance between the acceptor stem and the C-

terminal domain of SmpB[13] matches very closely the distance between the acceptor stem and the anticodon stem of tRNA[36] (Figure 7A), consistent with the hypothesis that SmpB plays the role of the anticodon arm in tmRNA.[13–15]

Recent cryo-EM studies have shown a large conformational rearrangement taking place in the tmRNA structure while the first MLD codon interacts with the A site (Figure 7B).[37–39] These studies show that during accommodation helix H2 and pk1 move all together towards the intersubunit space, while pk2 remains in place. This movement may assist placing the region upstream of the open reading frame in contact with SmpB to position the resume codon into the A site of the stalled ribosome.[39] The $Mg^{2+}$-dependent conformational change observed here may correspond to the rearrangement observed in the cryo-EM studies, suggesting that the structure and flexibility of the H2 arm plays an important role during tmRNA accommodation and translocation, perhaps in positioning pk1 and the MLD as the TLD moves through different sites in the ribosome. Altogether, our results may have interesting implications for the mechanism by which tmRNA replaces the defective mRNA by its own MLD.

## Supplementary Material

Refer to Web version on PubMed Central for supplementary material.

## Acknowledgments

We thank A. Buskirk for useful discussions, and critically reading this manuscript. S. Atapattu, N. Ban for the pET21 plasmid, R. Lamichhane for overexpressing SmpB, E. Aléman for assistance with the trFRET measurements and A. Brenlla for assistance with $R_0$ determination.

**Funding.** The Rueda lab is funded by the NIH [R01GM085116] and a CAREER award from the NSF [MCB0747285].

## Abbreviations

| | |
|---|---|
| **tmRNA** | transfer-messenger RNA |
| **tmRNAΔ** | truncated tmRNA derivative lacking nucleotides 83–326 |
| **tRNAΔ** | truncated tRNA missing the anticodon loop |
| **mtRNAΔ** | truncated mitochondrial tRNA missing the anticodon loop |
| **SmpB** | Small binding protein B |
| **ssFRET** | steady-state Förster resonance energy transfer |
| **trFRET** | time-resolved Förster resonance energy transfer |
| **TLD** | tRNA like domain |
| **MLD** | mRNA like domain |

## References

1. Keiler KC. Biology of trans-translation. Annu Rev Microbiol. 2008; 62:133–151. [PubMed: 18557701]
2. Keiler KC. Physiology of tmRNA: what gets tagged and why? Curr Opin Microbiol. 2007; 10:169–175. [PubMed: 17383929]
3. Dulebohn D, Choy J, Sundermeier T, Okan N, Karzai A. Trans-Translation: The tmRNA-Mediated Surveillance Mechanism for Ribosome Rescue, Directed Protein Degradation, and Nonstop mRNA Decay. Biochemistry. 2007:46.

4. Moore SD, Sauer RT. The tmRNA system for translational surveillance and ribosome rescue. Annu Rev Biochem. 2007; 76:101–124. [PubMed: 17291191]
5. Withey JH, Friedman DI. A salvage pathway for protein structures: tmRNA and trans-translation. Annu Rev Microbiol. 2003; 57:101–123. [PubMed: 12730326]
6. Shi W, Zhang X, Jiang X, Yuan H, Lee JS, Barry CE 3rd, Wang H, Zhang W, Zhang Y. Pyrazinamide inhibits trans-translation in Mycobacterium tuberculosis. Science. 2011; 333:1630–1632. [PubMed: 21835980]
7. Zwieb C, Wower I, Wower J. Comparative sequence analysis of tmRNA. Nucleic Acids Res. 1999; 27:2063–2071. [PubMed: 10219077]
8. Karzai AW, Susskind MM, Sauer RT. SmpB, a unique RNA-binding protein essential for the peptide-tagging activity of SsrA (tmRNA). EMBO J. 1999; 18:3793–3799. [PubMed: 10393194]
9. Withey J, Friedman D. Analysis of the role of trans-translation in the requirement of tmRNA for lambdaimmP22 growth in Escherichia coli. J Bacteriol. 1999; 181:2148–2157. [PubMed: 10094693]
10. Ivanova N, Pavlov MY, Felden B, Ehrenberg M. Ribosome rescue by tmRNA requires truncated mRNAs. J Mol Biol. 2004; 338:33–41. [PubMed: 15050821]
11. Himeno H, Sato M, Tadaki T, Fukushima M, Ushida C, Muto A. In vitro trans translation mediated by alanine-charged 10Sa RNA. J Mol Biol. 1997; 268:803–808. [PubMed: 9180372]
12. Stagg SM, Frazer-Abel AA, Hagerman PJ, Harvey SC. Structural studies of the tRNA domain of tmRNA. J Mol Biol. 2001; 309:727–735. [PubMed: 11397092]
13. Bessho Y, Shibata R, Sekine S, Murayama K, Higashijima K, Hori-Takemoto C, Shirouzu M, Kuramitsu S, Yokoyama S. Structural basis for functional mimicry of long-variable-arm tRNA by transfer-messenger RNA. Proc Natl Acad Sci U S A. 2007; 104:8293–8298. [PubMed: 17488812]
14. Nonin-Lecomte S, Germain-Amiot N, Gillet R, Hallier M, Ponchon L, Dardel F, Felden B. Ribosome hijacking: a role for small protein B during trans-translation. EMBO Rep. 2009; 10:160–165. [PubMed: 19132006]
15. Miller MR, Liu Z, Cazier DJ, Gebhard GM, Herron SR, Zaher HS, Green R, Buskirk AR. The role of SmpB and the ribosomal decoding center in licensing tmRNA entry into stalled ribosomes. RNA. 2011; 17:1727–1736. [PubMed: 21795410]
16. Gutmann S, Haebel PW, Metzinger L, Sutter M, Felden B, Ban N. Crystal structure of the transfer-RNA domain of transfer-messenger RNA in complex with SmpB. Nature. 2003; 424:699–703. [PubMed: 12904796]
17. Lamichhane R, Daubner GM, Thomas-Crusells J, Auweter SD, Manatschal C, Austin KS, Valniuk O, Allain FH, Rueda D. RNA looping by PTB: Evidence using FRET and NMR spectroscopy for a role in splicing repression. Proc Natl Acad Sci U S A. 2010; 107:4105–4110. [PubMed: 20160105]
18. Sevenich FW, Langowski J, Weiss V, Rippe K. DNA binding and oligomerization of NtrC studied by fluorescence anisotropy and fluorescence correlation spectroscopy. Nucleic Acids Res. 1998; 26:1373–1381. [PubMed: 9490780]
19. Rueda D, Hsieh J, Day-Storms JJ, Fierke CA, Walter NG. The 5′ leader of precursor tRNAAsp bound to the Bacillus subtilis RNase P holoenzyme has an extended conformation. Biochemistry. 2005; 44:16130–16139. [PubMed: 16331973]
20. Walter F, Putz J, Giege R, Westhof E. Binding of tobramycin leads to conformational changes in yeast tRNA(Asp) and inhibition of aminoacylation. EMBO J. 2002; 21:760–768. [PubMed: 11847123]
21. Rueda D, Wick K, McDowell SE, Walter NG. Diffusely bound Mg2+ ions slightly reorient stems I and II of the hammerhead ribozyme to increase the probability of formation of the catalytic core. Biochemistry. 2003; 42:9924–9936. [PubMed: 12924941]
22. Walter NG. Structural dynamics of catalytic RNA highlighted by fluorescence resonance energy transfer. Methods. 2001; 25:19–30. [PubMed: 11558994]
23. Rueda D, Walter NG. Fluorescent energy transfer readout of an aptazyme-based biosensor. Methods Mol Biol. 2006; 335:289–310. [PubMed: 16785635]

24. Gondert ME, Tinsley RA, Rueda D, Walter NG. Catalytic core structure of the trans-acting HDV ribozyme is subtly influenced by sequence variation outside the core. Biochemistry. 2006; 45:7563–7573. [PubMed: 16768452]
25. Eis PS, Millar DP. Conformational distributions of a four-way DNA junction revealed by time-resolved fluorescence resonance energy transfer. Biochemistry. 1993; 32:13852–13860. [PubMed: 8268160]
26. Walter NG, Burke JM, Millar DP. Stability of hairpin ribozyme tertiary structure is governed by the interdomain junction. Nat Struct Biol. 1999; 6:544–549. [PubMed: 10360357]
27. Pereira MJ, Harris DA, Rueda D, Walter NG. Reaction pathway of the trans-acting hepatitis delta virus ribozyme: a conformational change accompanies catalysis. Biochemistry. 2002; 41:730–740. [PubMed: 11790094]
28. Hsieh J, Koutmou KS, Rueda D, Koutmos M, Walter NG, Fierke CA. A divalent cation stabilizes the active conformation of the B. subtilis RNase P x pre-tRNA complex: a role for an inner-sphere metal ion in RNase P. J Mol Biol. 2010; 400:38–51. [PubMed: 20434461]
29. Wower J, Zwieb CW, Hoffman DW, Wower IK. SmpB: a protein that binds to double-stranded segments in tmRNA and tRNA. Biochemistry. 2002; 41:8826–8836. [PubMed: 12102625]
30. Walter N. Probing RNA Structural Dynamics and UNIT 11.10 Function by Fluorescence Resonance Energy Transfer (FRET). Current protocols in Nucleic Acid Chemistry. 2002
31. Klostermeier D, Millar DP. Time-resolved fluorescence resonance energy transfer: a versatile tool for the analysis of nucleic acids. Biopolymers. 2001; 61:159–179. [PubMed: 11987179]
32. Bolton PH, Kearns DR. Effect of cations on tRNA structure. Biochemistry. 1977; 16:5729–5741. [PubMed: 338029]
33. Romer R, Hach R. tRNA conformation and magnesium binding. A study of a yeast phenylalanine-specific tRNA by a fluorescent indicator and differential melting curves. Eur J Biochem. 1975; 55:271–284. [PubMed: 1100382]
34. Jones CI, Spencer AC, Hsu JL, Spremulli LL, Martinis SA, DeRider M, Agris PF. A counterintuitive Mg2+-dependent and modification-assisted functional folding of mitochondrial tRNAs. J Mol Biol. 2006; 362:771–786. [PubMed: 16949614]
35. Saguy M, Gillet R, Metzinger L, Felden B. tmRNA and associated ligands: a puzzling relationship. Biochimie. 2005; 87:897–903. [PubMed: 16164997]
36. Sussman JL, Holbrook SR, Warrant RW, Church GM, Kim SH. Crystal structure of yeast phenylalanine transfer RNA. I. Crystallographic refinement. J Mol Biol. 1978; 123:607–630. [PubMed: 357742]
37. Weis F, Bron P, Giudice E, Rolland JP, Thomas D, Felden B, Gillet R. tmRNA-SmpB: a journey to the centre of the bacterial ribosome. EMBO J. 2010; 29:3810–3818. [PubMed: 20953161]
38. Weis F, Bron P, Rolland JP, Thomas D, Felden B, Gillet R. Accommodation of tmRNA-SmpB into stalled ribosomes: a cryo-EM study. RNA. 2010; 16:299–306. [PubMed: 20038631]
39. Fu J, Hashem Y, Wower I, Lei J, Liao HY, Zwieb C, Wower J, Frank J. Visualizing the transfer-messenger RNA as the ribosome resumes translation. EMBO J. 2010; 29:3819–3825. [PubMed: 20940705]

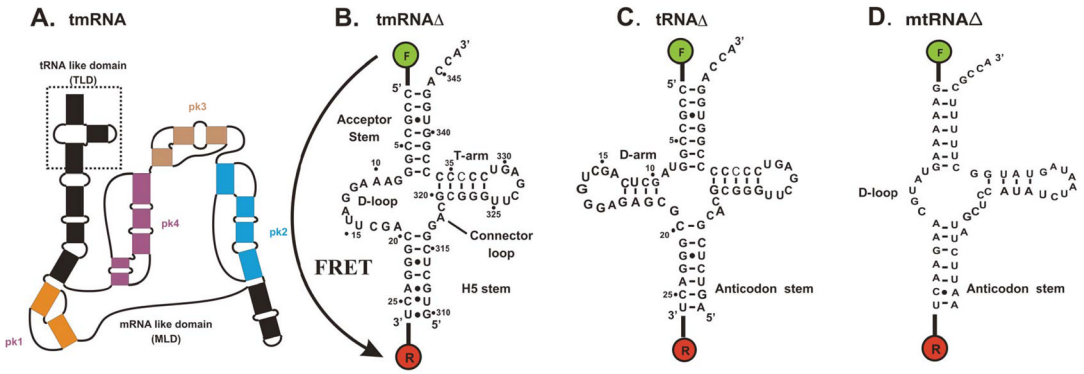


**Figure 1. Secondary structure of tmRNA and the fluorophore labeled constructs**

A. Secondary structure of tmRNA and location of the TLD and MLD. Four pseudoknots (pk1, orange; pk2, blue; pk3, brown; pk4, pink) connect the two major domains. B–D. Fluorescein (F) and tetramethylrhodamine (R) labeled constructs for FRET studies: tmRNAΔ (B), tRNAΔ (C) and mtRNAΔ (D).

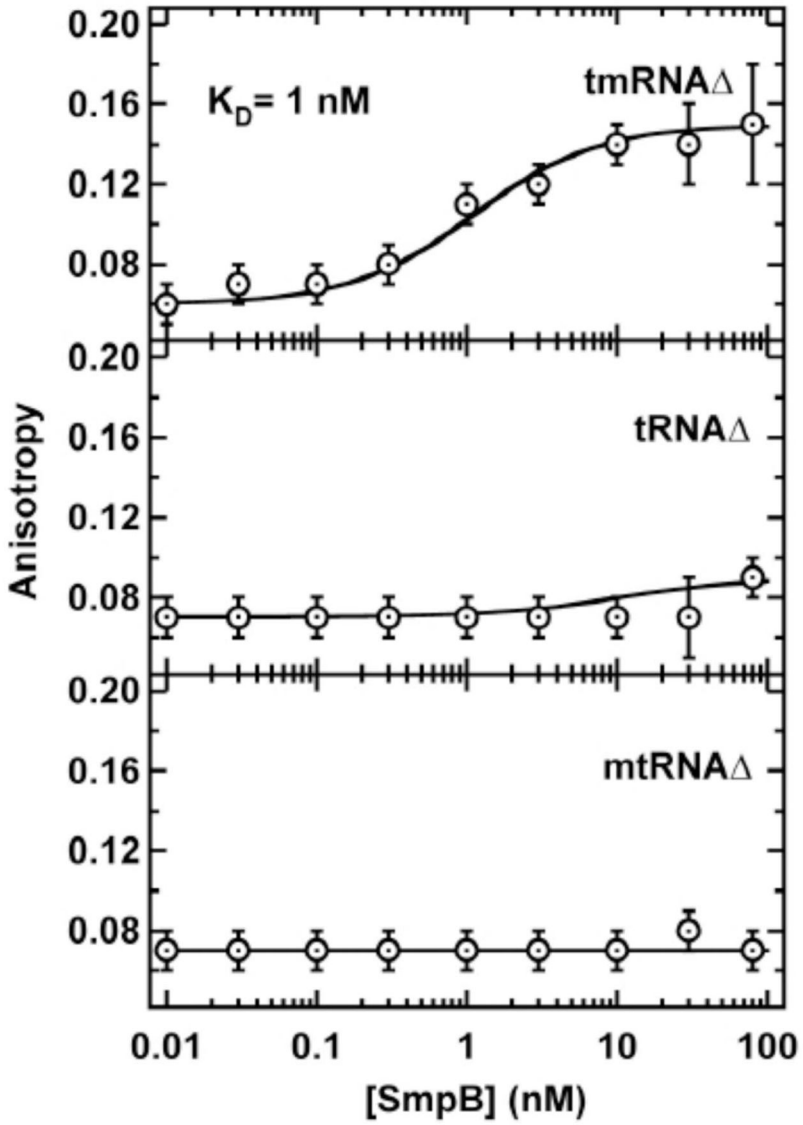


**Figure 2. SmpB binds tmRNA3 tightly and specifically**

Binding isotherms (50 mM Tris-HCl pH 7.5, 100 mM NaCl, 1 mM $MgCl_2$) between SmpB and tmRNAΔ (top), tRNAΔ (middle) and mtRNAΔ (bottom). Anisotropy increases indicate SmpB binding to the RNA. Only tmRNAΔ binds SmpB with a binding affinity $K_D$ = 1.0 ± 0.1 nM.

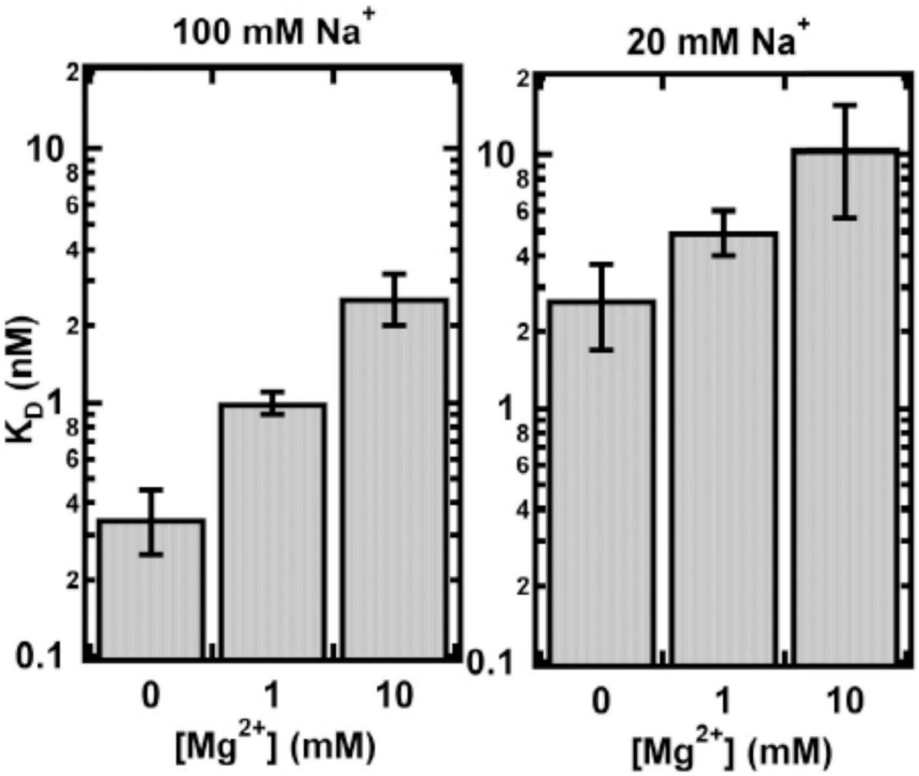


**Figure 3. Magnesium ions has an inhibitor effect on SmpB binding**

SmpB binding affinities ($K_D$) to tmRNAΔ as a function of $Mg^{2+}$ and $Na^+$ concentrations. Increasing $Mg^{2+}$ concentration causes a decrease in the SmpB binding affinity. Decreasing $Na^+$ concentration also decreases the SmpB binding affinity, and the $Mg^{2+}$ effect becomes less pronounced. Error bars stem from three independent measurements.

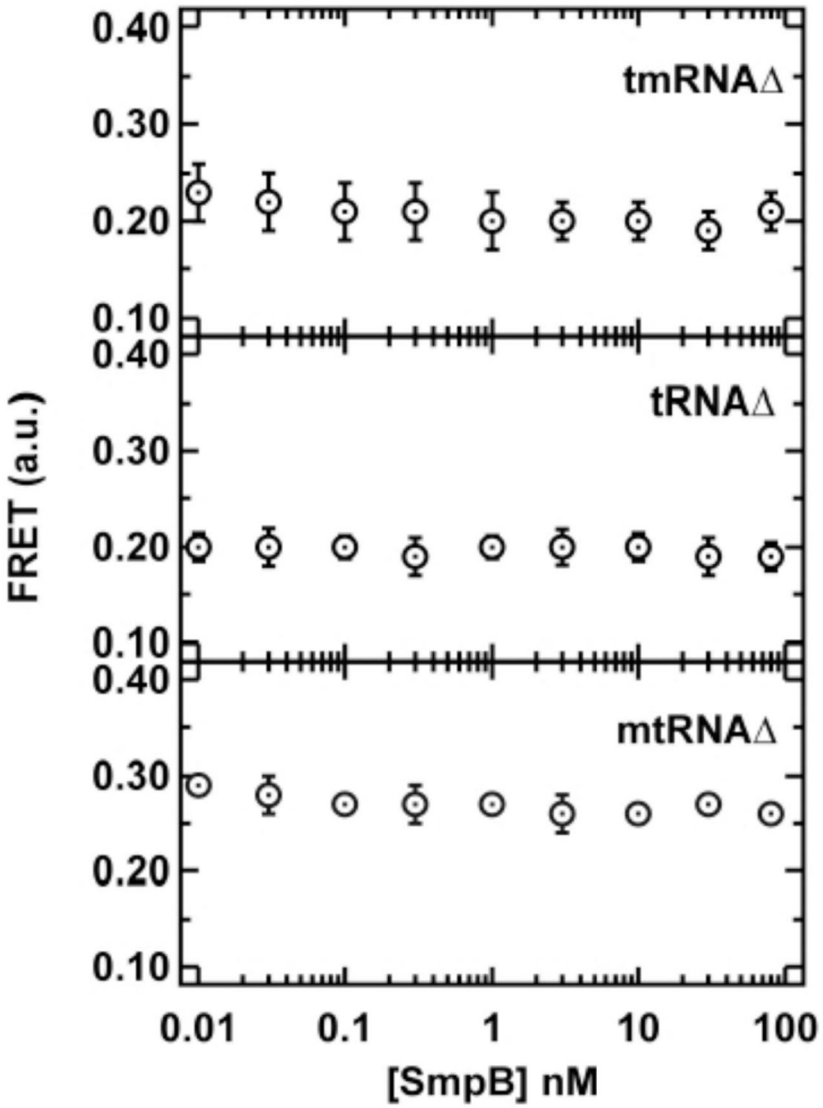


**Figure 4. The global structure of tmRNA3 does not change upon SmpB binding**

Apparent FRET efficiencies for the flurophore labeled tmRNAΔ (A), tRNAΔ (B) and mtRNAΔ (C) as a function of SmpB concentration. Error bars stem from three independent measurements. Apparent FRET efficiencies remain constant thorough out the titration range indicating that the global structure of tmRNAΔ does not change upon binding. Control RNAs (tRNAΔ and mtRNAΔ) are not expected to bind SmpB.

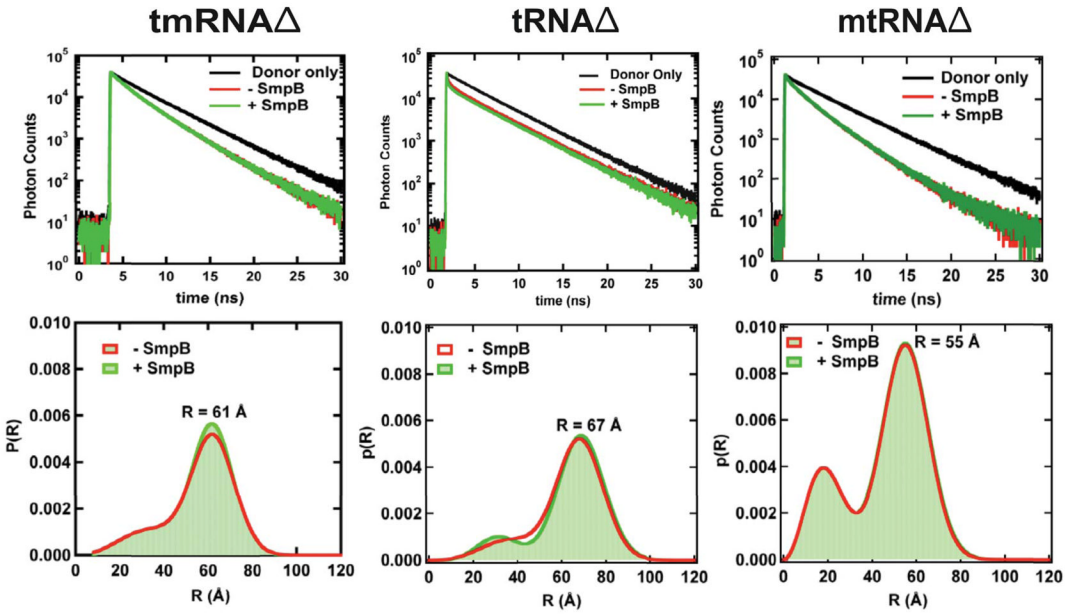


**Figure 5. Donor fluorescence decays and resulting distance distributions**

Top: Donor fluorescence decays in absence (black) and in presence of acceptor (red), and in presence of SmpB (green) for tmRNAΔ, tRNAΔ and mtRNAΔ, as indicated. Bottom: Distance distributions calculated using Förster's equation (see Materials and Methods) in absence (red) and presence (green) of SmpB. Results indicate that the global structure of tmRNAΔ does not change upon SmpB binding.

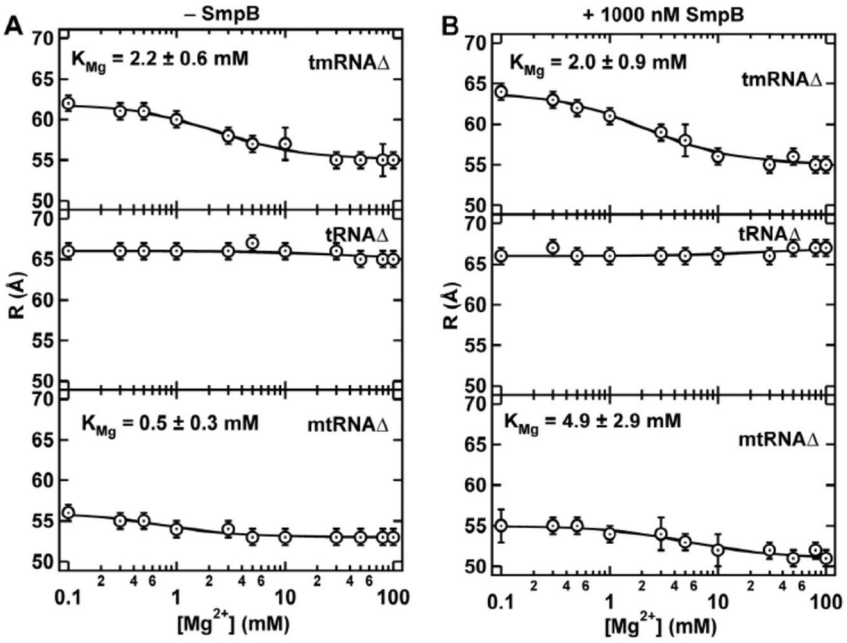


**Figure 6. Magnesium ions compress the structure of tmRNA3**

Donor-Acceptor distance measurement for tmRNAΔ (top), tRNAΔ (middle) and mtRNAΔ (bottom) in the absence (left) and presence (right) of saturating SmpB. A distance decrease is observed for tmRNAΔ and mtRNAΔ with increasing $Mg^{2+}$ concentration but not for tRNAΔ. Error bars stem from three independent measurements. The data was fit to the quadratic equation (see Methods).

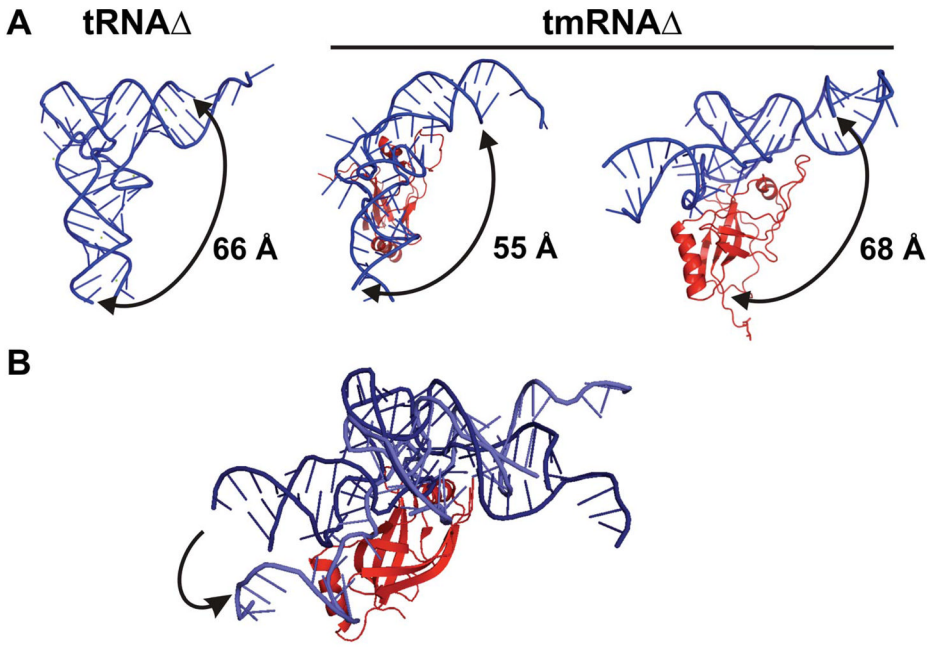


**Figure 7. Distance comparison and tmRNA-SmpB model inside stalled ribosome**

(A) Measured distances between the acceptor stem and the anti-codon stem in tRNAΔ and tmRNAΔ under saturating $Mg^{2+}$. The ~10 Å shorter distance in tmRNAΔ is consistent with the hypothesis that the H2a stem in tmRNA does not function as an anti-codon stem mimic during trans-translation. Based on the tmRNA-SmpB complex crystal structure,[13] the distance between the acceptor stem and the C-terminus of SmpB matches well with tRNAΔ. (B) Cryo-EM studies reveal a large amplitude conformational change in tmRNA.[37–39] The image is generated using images of the TLD-SmpB in the accommodated (dark blue PDB entry 3IZ4) and translocated states (light blue, PDB entry 3IYQ). Only the tRNA-like domains are shown for clarity. The two structures were aligned using SmpB as the reference. The arrow shows the conformational change consistent with the Mg-induced compaction observed here.